Evidence of elevation-dependent warming from the Chinese Tianshan Mountains

Lu Gao[1,2,3,4], Haijun Deng[1,2,3,4], Xiangyong Lei[3], Jianhui Wei[5], Yaning Chen[6], Zhongqin Li[7], Miaomiao Ma[8], Xingwei Chen[1,2,3,4], Ying Chen[1,2,3,4], Meibing Liu[1,2,3,4], Jianyun Gao[9]

[1]Institute of Geography, Fujian Normal University, Fuzhou 350007, China
[2]Fujian Provincial Engineering Research Center for Monitoring and Assessing Terrestrial Disasters, Fujian Normal University, Fuzhou 350007, China
[3]College of Geographical Sciences, Fujian Normal University, Fuzhou 350007, China
[4]State Key Laboratory of Subtropical Mountain Ecology (Funded by the Ministry of Science and Technology and the Fujian province), Fujian Normal University, Fuzhou 350007, China
[5]Institute of Meteorology and Climate Research (IMK-IFU), Karlsruhe Institute of Technology, Campus Alpine, Garmisch-Partenkirchen 82467, Germany
[6]State Key Laboratory of Desert and Oasis Ecology, Xinjiang Institute of Ecology and Geography, Chinese Academy of Sciences, Urumqi 830011, China
[7]State Key Laboratory of Cryospheric Sciences/Tianshan Glaciological Station, Northwest Institute of Eco-Environment and Resources, Chinese Academy of Sciences, Lanzhou 730000, China
[8]China Institute of Water Resources and Hydropower Research, Beijing 100038, China
[9]Fujian Key Laboratory of Severe Weather, Fuzhou 350001, China

Correspondence to: Lu Gao (l.gao@foxmail.com)

Abstract. The phenomenon in which the warming rate of air temperature is amplified with elevation is termed elevation-dependent warming (EDW). It has been clarified that EDW can accelerate the retreat of glaciers and melting of snow, which can have significant impacts on the regional ecological environment. Owing to the lack of high-density ground observations in high mountains, there is widespread controversy regarding the existence of EDW. Current evidence is mainly derived from typical high mountains such as the Swiss Alps, the Colorado Rocky Mountains, the Tropical Andes and the Tibetan Plateau/Himalayas. Rare evidence in other mountains has been reported, especially in arid regions. In this study, EDW features (regional warming amplification and altitude warming amplification) in the Chinese Tianshan Mountains (CTM) were detected using a unique high-resolution (1 km, 6-hourly) air temperature dataset (CTMD) from 1979 to 2016. The results showed that there were significant EDW signals at different altitudes on different time scales. The CTM showed significant regional warming amplification in spring, especially in March, and the warming trends were greater than those of continental China with respect to three temperatures (minimum temperature, mean temperature and maximum temperature). The warming rate of the minimum temperature in winter showed a significant elevation dependence ($p < 0.01$), especially above 4000 m. The greatest altitudinal gradient in the warming rate of the maximum temperature was found above 2500 m in April. For the mean temperature, the warming rates in January, February, and March showed prominent altitude warming amplification but with different significances. Within the CTM, the Tolm Mountains, the eastern part of the Borokoonu Mountains, the Bogda Mountains and the Balikun Mountains are representative regions that showed significant altitude

warming amplification on different time scales. This new evidence could partly explain the accelerated melting of snow in the CTM, although the mechanisms remain to be explored.

1 Introduction

Elevation-dependent warming (EDW) indicates that the warming rate of air temperature is amplified with elevation, especially in high mountain regions. Two basic characteristics regional warming amplification and altitude warming amplification are considered to be the "fundamental questions" of EDW by Rangwala and Miller (2012). Regional warming amplification means that the warming rate of air temperature in a certain mountain is greater than that in other regions outside this mountain. Altitude warming amplification means that the warming rate is greater in high-altitude areas than in low-altitude areas in the same mountain. Rangwala and Miller (2012) also concluded that the EDW exists in some typical mountains (e.g. Alps) because altitude warming amplification can be detected by observation and climate models. However, regional warming amplification is still difficult to detect because of the limited observations at the global scale. Therefore, to some extent, EDW could be determined once regional warming amplification or altitude warming amplification could be detected.

Owing to the high sensitivity of glaciers and snow to climate change, mountains are regarded as outposts of global climate change (Sorg et al., 2012). Previous studies have reported the potential widespread existence of the elevation-dependent warming (EDW) phenomenon, which is an ideal early indicator of climate warming in mountain systems under global climate change (Dong et al., 2015). EDW can accelerate the changes in mountain ecosystems, cryosphere systems, water cycles and biodiversity, leading to irreversible and profound impacts on the regional ecological environment and socioeconomic development (Mountain Research Initiative EDW Working Group, 2015; Rangwala and Miller, 2012). Therefore, the detection and exploration of the spatial and temporal differentiation characteristics of EDW play a crucial role not only in the in-depth understanding of regional climate change and in improving the predictive ability of mountain climate, but also in maintaining the relative stability and ecological balance of these natural mountain ecosystems.

Current evidence for the EDW phenomenon mainly stems from multi-source data detection and regional climate models. The main data resources include ground meteorological stations, radiosonde, reanalysis, and remote sensing data. For example, the warming rate has been found to be more intense in the high-altitude regions of Western Europe and Asia based on a global high-altitude observation dataset (Diaz and Bradley, 1997). The significant EDW phenomenon of the annual maximum and minimum temperatures in the Alps was detected based on ground observation sites (Beniston and Rebetez, 1996). The temperatures in the Alps at different altitudes showed distinctly different seasonal trends. The minimum temperature increases faster at high altitudes than at low altitudes (Jungo and Beniston, 2001). A significant EDW phenomenon for the annual mean temperature in tropical alpine areas was detected based on global radiosonde data (Seidel and Free, 2003). The warming trends for the maximum and minimum temperatures showed significant elevation dependence

in the 2000–4000 m altitude range of the Rocky Mountains (Diaz and Eischeid, 2007; Mcguire et al., 2012). The climate warming trends for the Qinghai-Tibet Plateau from 1961 to 1990 were proportional to altitude, especially in winter (Liu and Hou, 1998). In the high-altitude areas (above 4000 m) of the Qinghai-Tibet Plateau, the increment in the mean temperature over four seasons and on the annual scale is greater than that in the low-altitude areas (Du, 2001), and the temperature warming rate increases by 0.16 ℃ $10a^{-1}$ for every 1 km increment in altitude (Wang et al., 2012). An observation dataset containing 139 weather stations showed warmer trends at 4000 m (0.5 ℃ $10a^{-1}$) and 3000 m (0.357 ℃ $10a^{-1}$) than at 2000 m (0.316 ℃ $10a^{-1}$) with respect to the annual mean temperature in the Tibetan Plateau from 1961to 2012 (Yan and Liu, 2014). In general, from a regional perspective, the European Alps, Himalayan-Tibetan Plateau, South American Andes, and North American Rocky Mountains are hotspots for EDW studies (Wang et al., 2014; Thakuri et al., 2019; Guo et al., 2019; Pepin et al., 2019). From the perspective of the significance of EDW, the seasonal scale is more significant than the annual scale because of significant changes in climate drivers such as snow/ice cover, clouds and others at different elevations (Mountain Research Initiative EDW Working Group, 2015; Rangwala and Miller, 2012). Furthermore, the warming rate of the minimum temperature is greater than that of the maximum and mean temperatures (Rangwala and Miller, 2012; Mountain Research Initiative EDW Working Group, 2015).

Although many studies have detected EDW phenomena in different mountains globally, a widespread controversy still exists, and no consensus has been reached on the existence of EDW. This is mainly due to the scarcity of ground observation data, especially in mountains above 3000 m (Rangwala and Miller, 2012; Mountain Research Initiative EDW Working Group, 2015). Even the detection of EDW is different within the same mountain that uses different observations (i.e., different numbers of sites or different site locations). For example, some studies have shown a significant prevalence of EDW since the second half of the 20th century over the Tibetan Plateau (Liu et al., 2009; Rangwala et al., 2009). However, an analysis claimed that the EDW over the Qinghai-Tibet Plateau is not significant based on observations from 71 ground stations and 56 reanalysis grid (NCEP and ERA-40 grid with a spatial resolution of 2.5 °×2.5 °) data (You et al., 2010). Similarly, EDW has been found to be insignificant at altitudes above 5000 m based on observations from 25 ground stations and 0.5 ° grid data combined with WRF model simulations (Gao et al., 2018b). Although satellite data compensate for the deficiencies of ground observation stations to a large extent, the associated relatively short time series, long revisiting cycle, and image interpretation and inversion errors limit the reliability of EDW signal detection. It can be concluded that a uniform high-resolution air temperature dataset is the basic premise for accurate EDW detection.

As the farthest mountain system from the ocean, and the largest mountain system in arid regions of the world, the Tianshan Mountain system is extremely important for assessing climatic changes and the ecological environment in north-western China and the entire nation because of its special geographical location and complex terrain (Chen et al., 2016). As the "water tower" of Central Asia, the Tianshan Mountain system not only breeds many rivers, but also produces a unique desert oasis ecosystem (Sorg et al., 2012; Chen et al., 2016). There are approximately 9035 glaciers with an area of ~9225 km^2 and

of 1011 km^3 water resources in the Chinese Tianshan Mountains (CTM, Fig. 1) (Shi et al., 2009). However, recently, most glaciers in the CTM are in a state of accelerated degradation due to climate warming (Ding et al., 2006; Chen et al., 2016; Sorg et al., 2012). The warming rate in the CTM has reached 0.32–0.42 °C10a^{-1} in the past 50 years, which is much higher than the national average (Gao et al., 2018a; Xu et al., 2018). However, the EDW in the CTM still lacks systematic detection. Current research on climate warming in the CTM does not provide sufficient solid evidence for the EDW phenomenon. Therefore, in this study, EDW features in the CTM were comprehensively and systematically detected based on a unique high-resolution (1 km, 6-hourly) air temperature dataset (hereafter referred to as CTMD) (Gao et al., 2018a). The present study reveals the EDW characteristics for different temperature indicators at different time scales.

2 Data and Methods

2.1 CTMD

The lack of sufficient ground observations is the biggest obstacle in the accurate detection of the EDW phenomenon. This is one of the original intentions of the development of CTMD. Previous studies have shown that the ECMWF's third-generation reanalysis product, ERA-Interim, has a relatively small large-scale error (±2.5 K) and can capture the annual and seasonal climatologies very well (Gao et al., 2012, 2014, 2017; Simmons et al., 2010). Hairiguli et al (2019) concluded that the ERA-Interim could capture the inter-annual variations of monthly mean temperature in the CTM from via comparing with 45 observation sites from 1984 to 2016. Bai et al. (2013) also found that ERA-Interim temperature data are better than NCEP/NCAR data based on a comparison with nine observation sites in the CTM from 2004 to 2006. The system bias of ERA-Interim is mainly due to the height discrepancy between the ERA-Interim model height and observations (Gao et al., 2012, 2014, 2017). Thus, the bias could be significantly reduced for local climate trend investigations via an appropriate elevation correction procedure. A robust approach based on internal vertical lapse rates derived from different ERA-Interim pressure levels was developed to downscale the 0.25 ° grid ERA-Interim temperature to a 1 km grid derived from SRTM (Gao et al., 2018a). This scheme is fully independent of meteorological stations via Equation (1).

$$T_{1km} = T_{ERA\_025} + \Gamma \times \Delta h \quad (1)$$

T_{ERA_025} is the original 6-hourly ERA-Interim 2-m temperature at a 0.25 ° grid. Γ describes the ERA-Interim internal lapse rates derived from the temperatures and geopotential heights at different pressure levels. For example, Γ_{500_700} indicates the lapse rate between the 500 hPa and 700 hPa pressure levels, which is calculated by the temperature differences divided by geopotential height differences between these two pressure levels. Δh is the height difference between the ERA-Interim model height and the 1 km grid. Different Γ values were used according to the altitude of the 1 km grid. In other words, if the 1 km grid is lower than 1500 m in altitude, Γ_{850_925} is applied because the geopotential height between the 850 and 925 hPa pressure levels ranges from 150 m to 1500 m. If the grid altitude is higher than 4000 m, Γ_{500_600} is applied to the

downscaling model. The geopotential height at the 850 and 700 hPa pressure levels is the demarcation at altitudes of 1500 m and 3000 m, respectively. In total, four lapse rates (Γ_{500_600}, Γ_{600_700}, Γ_{700_850} and Γ_{850_925}) were used for different altitude ranges according to the 1 km grids (Gao et al., 2018a). Therefore, the unique high-resolution (1 km, 6-hourly) air temperature dataset (CTMD) for the Chinese Tianshan Mountains from 1979 to 2016 has a spatial resolution of 1 km (total 356133 grids) with 6-hourly time step at 00, 06, 12, and 18 UTC. More information regarding the downscaling scheme and on the CTMD can be found in Gao et al. (2012, 2017, 2018a).

Although, the CTMD was validated by 24 meteorological stations on a daily scale, indicating a high reliability for the climatology trend investigations, its limitations must be fully demonstrated. Whether the lapse rate accurately reflects the temperature changes at all altitudes is worth discussing. For example, the lapse rates of ERA-Interim are greater than those from September to December, whereas the lapse rate in the free atmosphere is steeper than that near the surface because of the different radiation mechanisms (Gao et al., 2018a). The lapse rate may be positive rather than negative because of the "Cold Lake" effect in winter, such as in the Turfan Basin, which may lead to a temperature inversion layer at night. In this situation, the downscaling model may be disabled during winter. Therefore, the opposite trend for minimum temperature during winter was captured by the CTMD compared to the slight positive warming trend from the 24 observation sites. Meanwhile, the trend of the diurnal temperature range (DTR) was not captured very well by the CTMD in spring and autumn (Gao et al., 2018a). We emphasise that the CTMD is only validated by 24 sites, which are mainly located in low terrains. Evaluating the credibility of the CTMD in the high peaks is difficult because few observations exist. Nevertheless, we believe that the CTMD is still creditable because it can capture the distribution characteristics of temperatures as well as the general warming trends.

2.2 CMA05

According to the two basic characteristics for the diagnosis of mechanisms responsible for EDW, regional warming amplification and altitude warming amplification were detected. The former feature is compared with those of other regions, such as plateaus, mountains, and low-altitude areas (basins and plains), to detect whether the warming trend in mountains is higher. The latter focuses on the warming trend differences within the mountains (e.g., different altitude ranges), which is to determine whether warming amplification in high-altitude areas is more significant than that in low-altitude areas. To detect the regional warming amplification, CMA05 was evaluated and compared with the CTMD.

The CMA05 dataset was obtained from the China Meteorological Data Sharing Service System of the National Meteorological Information Centre (http://data.cma.cn/data/cdcdetail/dataCode/SURF_CLI_CHN_TEM_MON_GRID_0.5.html). It contains three monthly temperature indices (minimum, mean and maximum temperature) at the 0.5 ° latitude-longitude grid. The CMA05 is highly reliable and has been widely applied in climatology studies since it was interpolated using the thin plate spline method based

on high-density ground stations (approximately 2400 national meteorological observation stations) since 1961. A common time period 1979–2016 was extracted for the current study. Previous studies found that the Qinghai-Tibetan Plateau (QTP) as the first step (highest) of China's terrain has a significant temperature warming trend over China (e.g. You et al., 2010). To reduce the influence of warming, the QTP was eliminated. Thus, not only the whole continental China (WCC), but the low-altitude areas (LCC), represented by excluding the CTM and the QTP from the WCC, were also used for comparison.

2.3 Snow cover and snow depth data

To further discuss the possible hypotheses and mechanisms with respect to EDW, snow cover and snow depth data in the CTM were collected. The snow cover rate was calculated by dividing the snow cover area by the total area. The snow cover area was interpreted based on the MODIS/Terra Snow Cover 8-Day L3 product (MOD10A2, version 5) with a 500 m spatial resolution from the NASA Snow and Glacier Data Centre (https://nsidc.org/data/MOD10A2/versions/5). The annual maximum and minimum snow cover rates in the CTM from 2002 to 2013 were calculated. This dataset was processed and provided by Chen et al. (2016) and Deng et al. (2019).

The daily snow depth data at a spatial resolution of 25 km from 1979 to 2016 over the CTM were derived from the National Earth System Science Data Centre, National Science & Technology Infrastructure of China (Che 2015). The snow depth was calculated based on the original daily passive microwave brightness temperature data (EASE-Grid) produced from SMMR (1979-1987), SSM/I (1987-2007) and SSMI/S (2008-2019) from the National Snow and Ice Data Centre (NSIDC). Detailed information on the data production can be found in studies of Che et al. (2008), Dai et al. (2015) and Dai et al. (2017).

2.4 Analytical methods

In this study, the 6-hourly data of the CTMD were aggregated to the minimum temperature (Tmin), maximum temperature (Tmax), and mean temperature (Tmean) on monthly, seasonal, and annual time scales. A standard linear regression was applied to calculate the warming rate in each grid from 1979 to 2016 for the CTMD and CMA05 datasets. The corresponding equation is given as follows:

$$y = \alpha x + \beta \quad (2)$$

where y is the temperatures (Tmin, Tmax and Tmean) on different time scales, x is the time series from 1979 to 2016, and the fitting coefficient (slope) α indicates the warming rate. Thus, in this study, EDW refers to the rate of warming over a multi-annual scale.

To detect the altitude warming amplification within the CTM, the entire altitude range was divided into 14 groups with 500 m intervals (Table 1). The numbers of grids in each group are listed in Table 1. Standard linear regression was also used to

assess different significance levels ($p < 0.1$, $p < 0.05$, $p < 0.01$, $p < 0.005$ and $p < 0.001$) of EDW for different altitude groups. In this analysis, y is the warming rate from 1979 to 2016 for each altitude group. The average warming rate of each group was used for the regression because of the different number of grids in each altitude group. Here, x denotes the 14 altitude groups (natural positive integers 1 to 14). Thus, the fitting coefficient (slope) represents the magnitude of the significance of EDW. The coefficients of determination (R^2) and confidence tests (p-values) illustrate the goodness of fit.

3 Results

3.1 Regional warming amplification of the CTM

The temperature trends on monthly, seasonal, and annual time scales with respect to Tmin, Tmax and Tmean were calculated using Eq. (2) based on the aggregated Tmin, Tmax and Tmean from 6-hourly CTMD data for each grid. Table 2 shows the ratio of the sum of grids at different significance levels ($p < 0.1$, $p < 0.05$ and $p < 0.01$) to the total grids (356133) with respect to monthly temperatures. All grids reached the significant levels for Tmax in March, followed by 99.35% of all grids for the Tmean. The number of grids that reached the significance level was the lowest in December, especially for Tmean and Tmax. For Tmin, more than half of the grids in only two months (March and June) reached the significance levels. For Tmean, five months (March, April, June, July and August) exceeded 50% grids at the significance levels. For Tmax, only February and March had more than half of all grids at the significance level. Although the temperature trend at some grids in a certain month did not reach a statistically significant level, it can still reflect climate warming to a certain extent. Thus, the subsequent analysis depends on the temperature trend of each grid.

The annual and seasonal temperature trends in the CTM were weaker than those over WCC with respect to the mean temperature (Tmean), maximum temperature (Tmax), and minimum temperature (Tmin), except during spring (Table 3). The warming rates in the Tmax and Tmin of spring both exceeded 0.6 ℃ $10a^{-1}$, which is much higher than that of WCC and LCC that represented by excluding the CTM and the QTP from the WCC. The summer Tmin and Tmean trends of CTM were also higher than those of LCC. The annual Tmin showed the greatest warming trend with a rate of 0.347 ℃ $10a^{-1}$, followed by Tmax and Tmean with warming rate of 0.323 and 0.245 ℃ $10a^{-1}$, respectively, in the CTM (Table 3). While summer had a much higher trend than autumn for Tmean and Tmin, it showed a comparable rate for Tmax (Table 3). Winter had the lowest rates compared with other seasons for the three temperature trends, with even a decreasing trend (−0.085 ℃ $10a^{-1}$) observed for Tmean. In general, Tmin and Tmax showed comparable rates in spring. A more significant increase in Tmin compared with Tmax was observed in summer and autumn. However, the trends of CTM were consistent with those of WCC and LCC, except for the winter Tmean (Table 3).

The warming rates vary from month to month, which is more significant than that from season to season. All temperature trends were negative in January and December in the CTM, which was different from that in the WCC and LCC (Table 4).

The rate of decrease was more significant in January than in December. Notably, Tmax decreased slightly in May, whereas Tmin warmed significantly at a rate of 0.624 ℃ $10a^{-1}$ in the CTM. The largest warming rates were observed for both the CTM and land surface of China in March for all temperature types. However, the CTM had a higher magnitude of warming. The warming trend was 1.339 ℃ $10a^{-1}$, which was almost double that over the whole of China (Table 4). Both rates exceeded 0.8 ℃ $10a^{-1}$ for Tmean and Tmin in the CTM in March. April showed the second largest Tmax and Tmean warming trends in the CTM, which were also higher than those over continental China. For Tmin, May and June had rates greater than 0.6 ℃ $10a^{-1}$. The significant warming trends from March to May resulted in higher trends in CTM than in continental China, especially in March (Table 4). In general, a more significant increment in Tmin was observed from March to June compared to that in other months. March and April showed remarkable warming trends for Tmax and Tmean (Table 4). In the entire CTM, Tmin increased faster than Tmax and Tmean. In general, regional warming amplification was significant in March and June at all temperatures. The trend for Tmax also increased faster in the CTM in February and April than over the entire land surface of China. The warming rates of Tmean and Tmin in the CTM were faster than those in the WCC and LCC in April and May, respectively. All temperature trends at different time scales in the WCC were higher than LCC, which implies that the warming rate of the Qinghai-Tibet Plateau contributes significantly to national warming.

3.2 Warming amplification with altitude within the CTM

The performances of different temperature types (Tmin, Tmean and Tmax) were diverse for different months. We selected the months with the most significant temperature warming trends to illustrate the complexity and variability of the EDW. To detect the altitude warming amplification features in the mountain areas, the CTM was divided into 14 groups with a 500 m altitude interval (Table 1). Notably, the temperature trends in the different elevation groups were significantly different than those of the entire CTM. Fig. 2 shows the Tmin trends at different elevations from 1979 to 2016 for four representative significant months (January, February, April, and December). As the number of grids in each elevation group is different, the boxplots show the interquartile range (25% to 75%) and median values. Meanwhile, linear regression was applied based on the average values, which indicated the altitude dependence of the warming trend (i.e. the significance of EDW). The monthly and seasonal temperature trends were calculated for each grid based on the averaged 6-hourly data. Thus, to maintain consistent trend calculation for the entire study, the average value was used for linear regression. In general, the EDW characteristics were significant for Tmin in January, February, April, and December. All lines of best fit are at the 0.001 significance level ($p < 0.001$). The temperature trends were positive at altitudes higher than 5000 m, with median values greater than 0 ℃ $10a^{-1}$ above 4000 m in January (Fig. 2a). The median values of most elevation groups were above the reference line in February, although the corresponding line of fit had a lower slope (0.033) compared with that of January (Fig. 2b). The 75% quartile ranges of the trends for all elevation groups in April were higher than 0 ℃ $10a^{-1}$ (Fig. 2c). All trends were positive for the regions above 4000 m in April. The prevalence of EDW was the most significant in December with the highest slope (0.064, $p < 0.001$). Although, most of lower altitude grids (< 4000 m) showed negative trends, the trends become positive at altitudes higher than 5000 m (Fig. 2d).

Although the slope (0.017) of the trend was not remarkable, a significant EDW trend ($p < 0.001$) was observed for Tmax in March (Fig. 3a). In contrast to April, August, and September, the same trend was observed for all elevation groups in March. Furthermore, all warming rates were greater than 0.8 ℃ $10a^{-1}$. Significant elevation-dependent cooling was observed in the altitude range of 0–2500 m for Tmax in April. However, the temperature warming rate increased sharply (slope = 0.069, $p <$ 0.001) with increasing altitude from 2500 m to 7100 m. The median values were higher than 0.4 ℃ $10a^{-1}$ (Fig. 3b). Similar to April, EDW begins at a height of 4000–4500 m in August and September. However, the warming rates were greater in September with the most positive values compared to August (Figs. 3c and 3d). In general, while Tmax warming is not widespread, it is more significant at higher elevations.

For Tmean, the EDW trend was most significant in January with the highest significance level (slope = 0.036, $p < 0.001$, Fig. 3a). However, the warming rates in January were only slightly above 0 ℃ $10a^{-1}$ at higher elevations. Although February and March also showed significant EDW at the 0.005 and 0.05 significant levels, respectively, the warming rates were much higher in March than in February with an average median value of approximately 0.8 ℃ $10a^{-1}$ (Figs. 4b and 4c). Significant EDW occurred above an elevation of 4500 m in August (slope=0.037, Fig. 4d). Table 5 summarises the monthly temperature trends over different elevations based on CTMD from 1979 to 2016, especially the significant trend at higher elevations, as shown in Figs. 2 to 4. The performances for all months and seasons are also provided in the supplementary material (Fig. S1-S13).

3.3 Spatial distribution pattern of the warming trend over the CTM

To better detect altitude warming amplification, four typical zones with high mountains (above 3000 m) were selected: Zone 1 (represented by the Tolm Mountains), Zone 2 (central Tianshan, including the eastern part of the Borokoonu Mountains), Zone 3 (represented by the Bogda Mountains), and Zone 4 (represented by the Balikun Mountains) (Fig. 5). The monthly minimum temperature trends of January in the higher altitude mountains were greater than those in the surrounding LCCs,, especially in Zones 3 and 4 (Fig. 5a). The highest warming trend (exceeding 1.0 ℃ $10a^{-1}$) was observed around the eastern Bogda Mountains (above 3000 m) in Zone 3. The lowlands to the north of the Bogda Mountains showed a cooling trend (Fig. 5a). Zone 4 also showed a remarkable EDW phenomenon (0.3–0.6 ℃ $10a^{-1}$), wherein high mountains such as the Balikun were slightly warmer than the surrounding lowlands. Although the warming trend of Zone 1 was not as distinct as that of Zones 3 and 4, compared with the Ili Valley (cooling trend), the warming rate was still remarkable (~0.4 ℃ $10a^{-1}$). In December, the warming trend was more significant in Zone 1 than in the other zones (Fig. 5b). The trend in the Tolm Mountains (exceeding 0.4 ℃ $10a^{-1}$) was much higher than that in the Ili Valley (cooling trend), which is located in the northern part of Zone 1. The warming rate at high altitudes in Zone 3 was higher (0.2–0.4 ℃ $10a^{-1}$) than that in the lowlands. There was no obvious warming amplification in the high-altitude mountains of Zone 4 to the low-altitude areas (Fig. 5b). However, it is worth noting that even in the same mountainous areas, such as in the Bogda Mountains in Zone 3, the warming rate in the east was notably higher than that in the northwest. In addition, to more intuitively reveal that the

warming rate of temperature was amplified with elevation, a southwest-southeast direction terrain profile was created for Zone 2 as an example. It is clear that the minimum temperature warming trends accelerated as the elevation increased in January and December. The warming trends become positive at an altitude of approximately 3000 m (Fig. 5).

The maximum temperature in March in the entire CTM significantly increased with rates ranging from 0.9 to 2.0 ℃ $10a^{-1}$ (Fig. 6a). The highest warming rate was observed in western Ili Valley. However, all typical zones showed strong altitude-warming amplification features. The areas above 4500 m in Zone 1 showed trends higher than 1.4 ℃ $10a^{-1}$. The smoothed contour at 3000 m corresponds to a distinct boundary in Zone 2. The temperature warming rates were almost higher than ~1.5 ℃ $10a^{-1}$ in the areas above 3000 m, whereas the rates were smaller in the low altitude areas (Fig. 6a). The sub-plots illustrate consistent trends between the elevation and maximum temperature in Zone 2 (Fig. 6a). The trend was higher than ~1.1 ℃ $10a^{-1}$ in March, whereas the trend became positive at approximately 2000 m in September (Fig. 6b). The difference between the warming rates in the high-altitude areas and low-altitude areas was the most remarkable in Zone 3. The temperature warming trend on the hilltop of the Bogda Mountains was much higher than that at the foot of the mountains (Fig. 6a). The temperature warming rate in Zone 4 ranged from 1.3 to 1.6 ℃ $10a^{-1}$. The trend differences between the high-altitude areas and low-altitude areas in Zone 4 were not as remarkable as those in Zone 3 (Fig. 6a). However, the warming rate on the hilltop was much higher than that in the neighbouring lowlands (Fig. 6a).

The spatial distribution of the maximum temperature in September showed distinctive east-west differentiation. The warming rates in Zones 3 and 4 were greater than those in Zones 1 and 2 (Fig. 6b). The EDW features were not notable in Zone 4. In contrast, the temperature in the high-altitude areas showed a slower warming trend (approximately 0.2–0.3 ℃ $10a^{-1}$) than that in the low-altitude areas in Zone 3 (Fig. 6b). A slight EDW phenomenon was observed in the Tolm Mountains in Zone 1. However, Zone 2 showed remarkable EDW in September compared to that in the other zones. Similar to March, areas above 3000 m warmed faster than the lowlands, especially in the Ili Valley (Fig. 6b). In summary, Zone 2 was found to have a significant EDW area at the maximum temperature for March and September.

Zones 1 and 4 tended to exhibit the altitude warming amplification phenomenon for the monthly mean temperature in January (Fig. 7a). The temperature decreased (by approximately −0.2 to −0.4 ℃ $10a^{-1}$) in the Ili Valley but increased (approximately 0.05 to 0.15 ℃ $10a^{-1}$) in the Tolm Mountains, especially in the high-altitude areas (Fig. 7a). Zone 4 warmed faster than regions outside the zone. However, the warming trend was not notable in the high-elevation areas compared with that in the lowlands within this zone (Fig. 7a). The temperatures showed cooling trends in Zones 2 and 3. Nevertheless, the trend was amplified with an elevation in January in Zone 2. The high-altitude areas were warmer than the low-altitude regions, especially in the Bogda Mountains of Zone 3 (Fig. 7a). The spatial distribution of the warming rate in February was similar to that in January. However, the trend in most areas of the CTM was positive (Fig. 7b). Zones 3 and 4 showed obvious EDW phenomena in February. The difference between the temperature warming rates in the high and low terrains of these two zones exceeded 0.2 ℃ $10a^{-1}$. The trend in the high terrain of Zone 2 was greater than that in the valleys in the

western part of the zone (eastern Ili Valley). However, the temperature in the south of the zone warmed faster than that in the high mountains in the northern part of Zone 2 (Fig. 7b). The temperature warming rate continuously increased in the altitude gradient along the terrain profile in Zone 2 in February (Fig. 7b). The southwestern Tolm Mountains in Zone 1 warmed up faster than the north-eastern mountains. In general, the warming trend of the mean temperature was not as dramatic as that of the minimum and maximum temperatures in the CTM. The spatial distribution of warming trends for all months and seasons can be found in the supplementary material (Fig. S14 – S30).

4 Discussion

Our analysis shows that the EDW phenomenon is very complicated for a large mountain system. It is difficult to arbitrarily judge the prevalence of EDW in mountain systems. Based on a comprehensive quantitative analysis, we believe that significant EDW signals exist in the CTM on local scales with respect to different temperature types. Although previous studies have mainly focused on the EDW of annual and seasonal temperatures, the monthly scale has not received sufficient attention. However, seasonal temperatures do not clearly reflect the EDW characteristics. In complex terrains, monthly temperature changes are more significant, especially during seasonal transitions. For example, rapid warming in March would accelerate the melting of ice and snow, affecting glaciers and regional water resources in the mountains.

The air temperature changes were mainly affected by two aspects: one is the vertical energy exchange between the ground and atmosphere, which leads to periodic changes on the daily and annual scales; and the other is the temperature advection caused by movement of cooling and heating masses, which leads to non-periodic changes. Numerous studies have shown that atmospheric circulation not only affects the latitude and zonality of climate via the zonal distribution of circulation but also expands the influence range of sea-land and topography via energy and water transportation (Dickinson, 1983; Harding et al., 2001). It is worth noting that the temperature trend is always positive at an altitude of 4500 m or higher in the CTM. However, the temperature has a cooling trend in winter below 3000 m, especially in Tmin (Fig. 2). The significant altitude warming amplification phenomenon could only be observed above 4500 m for the Tmean in August (Fig. 3 and Table 5). The air at high altitudes is similar to that in the free atmosphere and the dry adiabatic process is dominant. The absorption and reflection of solar radiation by the surface mainly determine the temperature change. In low-altitude areas, the impact of the underlying surface characteristics (e.g. terrain and land cover) is more significant. The CTM has a complex terrain with many mountain basins and canyons. Because of the “Cold Lake” effect in winter, the lapse rate is even positive. A temperature inversion layer often occurs in deep canyons at night. Meanwhile, in low-altitude areas, the more surface soil moisture results in an increase in the latent heat fluxes, which further causes more absorbed solar radiation and then temperature warming in winter (Rangwala et al., 2012). This mechanism is closely related to snowlines and treelines because the migration of snowlines and treelines changes the surface albedo (Mountain Research Initiative EDW Working Group, 2015).

On a local scale, the ice and snow albedo, cloud cover, water vapour and radiation flux, and aerosols (including black carbon) are considered to be the main factors influencing EDW (Mountain Research Initiative EDW Working Group, 2015; Rangwala and Miller, 2012). However, irrespective of clouds, water vapour, and aerosols, the core mechanism is that they affect the absorption of solar short-wave radiation by the land surface and long-wave radiation outward from the land surface (Shi et al., 2020; Zhang et al., 2018). The balance of surface energy changes leading to increasing/decreasing near-surface air temperature. In other words, the surface energy balance is the key mechanism that affects seasonal and interannual changes in EDW (Rangwala and Miller, 2012).

Surface albedo is a comprehensive indicator of many factors that affect surface energy balance. It is also the core factor and key variable that controls the surface energy budget (Dickinson, 1983; Harding et al., 2001; Wang et al., 2005). Numerous factors such as terrain, vegetation cover, ice and snow, soil moisture, soil physical properties, and meteorological conditions affect surface albedo (Zhang et al., 2018). For high mountain regions, vegetation cover and ice/snow cover are the two most important factors (Dickinson, 1983; Zhang et al., 2016; Zhang et al., 2018). For the entire CTM, small glaciers are more sensitive to the warming climate. The estimated glacier mass loss could be -2.3×10^{3} kg m^{-2} below 3000 m, especially in Zone 2 (Deng et al., 2019). The snow cover and its duration also show a decreasing trend (Sorg et al., 2012; Deng et al., 2019). Guo and Li (2015) found a decreasing trend in the ratio of snowfall to precipitation (S/P) in the CTM, especially in the four typical zones (Zones 1 to 4) in this study.

Deng et al. (2019) found that the snow cover rate in the CTM decreased at a rate of 0.44% from 2002 to 2013. According to the snow cover rate data from Chen et al. (2016) and Deng et al. (2019), the maximum snow cover rate always occurred in January, whereas the minimum snow cover occurred in July. We tested the relationship between monthly Tmin, Tmean and Tmax with the maximum/minimum snow cover rate for each month from 2002 to 2013. Figure 8 shows the relationship between the temperature and snow cover rate. Only the Tmin in February had a strong correlation ($R^2 = 0.302$, $p < 0.1$) with the maximum snow cover rate (Fig. 8a). For the minimum snow cover rate, Tmax in August showed a significant correlation ($R^2 = 0.256$, $p < 0.1$) (Fig. 8a). The correlation between temperature in other months and the snow cover rate was not significant (not shown here).

The annual trend of snow depth over the CTM from 1979-2016 was -0.12 cm $10a^{-1}$, which means that the melting of snow is accelerating. Except January (0.16 cm $10a^{-1}$) and February (0.05 cm $10a^{-1}$), the reduction in snow depth in other months ranged from -0.01 to 0.58 cm $10a^{-1}$. The snow depth reduced the fastest in March with a rate of -0.58 cm $10a^{-1}$, followed by April with a rate of -0.45 cm $10a^{-1}$. Thus, spring had the highest decreasing trend of snow depth. However, the temperature warming trends were most significant in spring and March with respect to Tmin, Tmean and Tmax (Tables 3 and 4). The relationship between snow depth and temperature was further investigated in the CTM from 1979 to 2016 (Table 6). A significant correlation ($p < 0.01$) was found between Tmin and snow depth in March and June. For the couple of Tmean and snow depth, a remarkable correlation ($p < 0.01$) was also found in March, June and August, respectively. The significant

correlation ($p < 0.01$) was observed only in December between Tmax and snow depth (Table 6). In cold months, for example, November and January, a relatively significant correlation ($p < 0.05$) was found between Tmean/Tmax and snow depth. Figure 9 shows the scatter plots of the comparison of Tmin and Tmean in March with the snow depth. A negative correlation was perspicuous and visible. In general, there was a negative correlation between temperature and snow cover/snow depth (Figs. 8 and 9), which implies that temperature warming promotes the accelerated melting of snow. Meanwhile, the accelerated melting of snow may affect temperature warming. The detailed feedback mechanism between snow and temperature needs to be further verified and explored using advanced technology and models. In summary, although many hypothetical mechanisms of EDW have received widespread attention, most of them are limited to phenomenon description and qualitative analysis. The present study attempted to conduct preliminary explorations of the mechanism based on limited snow cover and snow depth data. There is a lack of quantitative investigations on the core processes, dominant factors, and spatio-temporal differences of EDW.

5 Conclusions

Compared with the warming trend over the national land surface (WCC) and the low-altitude areas (LCC), the CTM is warming faster (0.633 and 0.640 ℃ $10a^{-1}$ for Tmin and Tmax, respectively) in spring (Table 3). However, on a monthly scale, warming rates are more complicated. The warming trends of the three temperature indicators (Tmin, Tmax, and Tmean) in March (0.835 and 1.339 ℃ $10a^{-1}$ for Tmin and Tmax, respectively) and June (0.752 and 0.422 ℃ $10a^{-1}$ for Tmin and Tmax, respectively) in the CTM were higher than those over the entire national land surface on an average (Table 4). In addition, Tmax in February, Tmax and Tmean in April, and Tmin in May were also higher than the national average. Therefore, EDW detection based on at monthly scale was more reasonable and accurate.

It cannot be simply concluded that the high-altitude areas are warming faster than the low-altitude areas. Quantitative analysis is required to provide solid evidence for the EDW phenomenon. Using altitude grouping and a linear regression model, we quantitatively determined the significance of EDW along with the detailed performance of the warming trends with respect to Tmin, Tmean and Tmax at different altitudes. In the case of Tmin, January, February, April, and December showed significant EDW trends ($p < 0.001$). The most significant EDW phenomenon was found in December (Table 5). In other words, Tmin was associated with a strong EDW in winter. The warming rates of Tmin above 5000 m were always positive, which could lead to faster melting of snow. March, April, August, and September showed different elevation-based sensitivities with respect to Tmax. However, a significant EDW phenomenon can only be found at altitudes above 2500 m, 4000 m, and 4500 m in April, August, and September, respectively. The Tmax warming trends in March and April were always positive in the CTM. The cold months from January to March showed significant EDW phenomena over the entire CTM with respect to Tmean. In August, EDW was detected in areas higher than 4500 m.

The CTM is a large mountain system comprising many mountains. Therefore, EDW characteristics are diverse in different mountains. The EDW of Tmin in January was significant in the Bogda and Balikun Mountains, whereas it was significant in December in the Tolm Mountains (Fig. 5). For Tmax in March, all typical mountains exhibited EDW characteristics, especially the central CTM and Bogda Mountains (Fig. 6). A significant EDW signal of Tmax was observed in September in central CTM (eastern part of the Borokoonu Mountains). The most significant EDW signal of Tmean was observed in the Tolm and Balikun Mountains in January. The Bogda and Balikun Mountains exhibited significant EDW features in February.

After preliminary research, a significant negative correlation (p<0.001) between minimum/mean temperature and snow depth was observed in March and June (Fig. 9). However, the specific feedback mechanism between snow and temperature remains unclear. Even in the same mountainous area, significantly different mechanisms of EDW were observed for different topographies, altitudes, and seasons. Future studies should focus on conducting in-depth quantitative research on the mechanism of EDW based on regional climate models and field surveys, especially in Zones 1 and 2 with accelerating snow melting.

6 Data availability

The dataset is released at https://doi.org/10.1594/PANGAEA.887700 in the Network Common Data Form (NetCDF) format. The coverage of the dataset is 41.1814-45.9945 °N, 77.3484-96.9989 °E. The spatial resolution is 1km and the total number of grid points is 818126 for the larger Chinese Tianshan Mountain region, which includes more surrounding areas. This study used 356133 grids. The time step was 6-hourly at 00, 06, 12, and 18 UTC. The dataset contains 288 NetCDF files and one user guidance file. The monthly temperature data set at the 0.5 ° latitude-longitude grid (CMA05) over continental China was provided by the China Meteorological Data Sharing Service System of the National Meteorological Information Center (http://data.cma.cn/data/cdcdetail/dataCode/SURF_CLI_CHN_TEM_MON_GRID_0.5.html, last access: 05 January 2021). The MODIS/Terra Snow Cover 8-Day L3 product (MOD10A2, version 5) for snow cover rate calculation was provided by the NASA Snow and Glacier Data Centre (https://nsidc.org/data/MOD10A2/versions/5, last access: 07 January 2021). The daily snow depth data were provided by the National Earth System Science Data Centre, National Science & Technology Infrastructure of China (http://www.geodata.cn, 05 January 2021).

Author contributions

L.G. designed the research and collected the data, H.D., X.L. and J.W. contributed to the data processing and analysis, L.G. wrote the manuscript, and M.M., X.C., Y.N.C., Z.L., J.G., Y.C. and M.L. contributed to the discussion.

Competing interests

The authors declare that they have no conflict of interest.

Additional information

More analysis figures could be found in the Supplementary material.

Acknowledgements

This study was supported by the National Key Research and Development Program (2018YFE0206400 and 2018YFC1505805), the National Natural Science Foundation of China (41501106, 41877167 and 41807159), the Research and Development Support Program of the China Institute of Water Resources and Hydropower Research (IWHR) (JZ0145B582017), the Scientific Projects from Fujian Provincial Department of Science and Technology (2019R1002-3), and the Outstanding Young Scientific Research Talents Cultivation Program, Education Department of Fujian Province. Dr. Jianhui Wei was supported financially by the German Research Foundation through funding of the AccHydro project (DFG-Grant KU 2090/11-1).

References

Bai, L., Wang, W., Yao, Y., Ma, J., and Li, L.: Reliability of NCEP/NCAR and ERA-Interim Reanalysis Data on Tianshan Mountainous Area, Desert and Oasis Meteorology, 7(6): 51-56, 2013. (In Chinese)

Beniston, M., and Rebetez, M.: Regional behavior of minimum temperatures in Switzerland for the period 1979-1993, Theoretical and Applied Climatology, 53, 231-243, 1996.

Che, T.: Long-term series of daily snow depth dataset in China (1979-2019), National Tibetan Plateau Data Center, 2015. DOI: 10.11888/Geogra.tpdc.270194. CSTR: 18046.11.Geogra.tpdc.270194.

Che, T., Li, X., Jin, R., Armstrong, R., and Zhang, T.J.: Snow depth derived from passive microwave remote-sensing data in China, Annals of Glaciology, 49, 145-154, 2008.

Chen, Y., Li, W., Deng, H., Fang, G., and Li, Z.: Changes in Central Asia's water tower: past, present and future, Scientific Reports, 6, 35458, 10.1038/srep35458, 2016.

Dai, L.Y., Che, T., and Ding, Y.J.: Inter-calibrating SMMR, SSM/I and SSMI/S data to improve the consistency of snow-depth products in China, Remote Sensing, 7(6), 7212-7230, 2015.

Dai, L.Y., Che, T., Ding, Y.J., and Hao, X.H.: Evaluation of snow cover and snow depth on the Qinghai–Tibetan Plateau derived from passive microwave remote sensing, The Cryosphere, 11(4), 1933-1948, 2017.

Deng, H., Chen, Y., and Li, Y.: Glacier and snow variations and their impacts on regional water resources in mountains, Journal of Geographical Sciences, 29(1): 84-100, 2019.

Diaz, H. F., and Bradley, R. S.: Temperature variations during the last century at high elevation sites, Climatic Change, 36, 253-279, 1997.

Diaz, H. F., and Eischeid, J. K.: Disappearing "alpine tundra" Köppen climatic type in the western United States, Geophysical Research Letters, 34, 2007.

Ding, Y., Liu, S., Li, J., and Shangguan, D.: The retreat of glaciers in response to recent climate warming in western China, Annals of Glaciology, 43, 97-105, 2006.

Dickinson, R. E.: Land surface processes and climate-surface albedos and energy balance, Advances in Geophysics, 25: 305-353, 1983.

Dong, D., Huang, G., Qu, X., Tao, W., and Fan, G.: Temperature trend–altitude relationship in China during 1963–2012, Theoretical and Applied Climatology, 122, 285-294, 2015.

Du, J.: Change of temperature in Tibetan Plateau from 1961 to 2000, Acta Geographica Sinica, 56, 682-690, 2001. (in Chinese)

Gao, L., Bernhardt, M., and Schulz, L.: Elevation correction of ERA-interim temperature data in complex terrain, Hydrology and Earth System Sciences, 16(12): 4661-4673, 2012.

Gao, L., Hao, L., and Chen, X.W.: Evaluation of ERA-interim monthly temperature data over the Tiberan Plateau, Journal of Mountain Science, 11(5): 1154-1168, 2014

Gao, L., Bernbardt, M., Schulz, K., and Chen, X.W.: Elevation correction of ERA-Interim temperature data in the Tibetan Plateau, International Journal of Climatology, 37(9): 3540-3552, 2017.

Gao, L., Wei, J., Wang, L., Bernhardt, M., Schulz, K., and Chen, X.: A high-resolution air temperature data set for the Chinese Tian Shan in 1979–2016, Earth System Science Data, 10, 2097-2114, 2018a.

Gao, Y., Chen, F., Lettenmaier, D. P., Xu, J., Xiao, L., and Li, X.: Does elevation-dependent warming hold true above 5000 m elevation? Lessons from the Tibetan Plateau, npj Climate and Atmospheric Science, 1, 2018b.

Hairiguli, N., Yusufujiang, R., Madiniyati, D., and Roukeyamu, A.: Adaptability Analysis of ERA-Interim and GHCN-CAM Reanalyzed Data Temperature Values in Tianshan Mountains Area，China，Mountain Research, 37(4): 613-621, 2019. (In Chinese)

Harding, R.J., Gryning, S.E., Halldin, S., and Lloyd, C.R.: Progress in understanding of land surface/atmosphere exchanges at high latitudes, Theoretical and Applied Climatology, 70, 5-18, 2001.

Mountain Research Initiative EDW Working Group: Elevation-dependent warming in mountain regions of the world, Nature Climate Change, 5, 424-430, 2015.

Guo, L., and Li, L.: Variation of the proportion of precipitation occurring as snow in the Tian Shan Mountains, China, International Journal of Climatology, 35, 1379-1393, 2015.

Guo, D., Sun, J., Yang, K., Pepin, N., and Xu, Y.: Revisiting recent elevation-dependent warming on the Tibetan Plateau using satellite-based data sets, Journal of Geophysical Research, 124, 8511-8521, 2019.

Jungo, P., and Beniston, M.: Changes in the anomalies of extreme temperature anomalies in the 20thcentury at Swiss climatological stations located at different latitudes and altitudes, Theoretical and Applied Climatology, 69, 1-12, 2001.

Liu, X., and Hou, P.: Relationship between the climatic warming over the Qinghai -Xizang Plateau and its surrounding areas in recent 30 years and the elevation, Advances in Climate Change Research, 017, 245-249, 1998. (in Chinese)

Liu, X., Cheng, Z., Yan, L., and Yin, Z.: Elevation dependency of recent and future minimum surface air temperature trends in the Tibetan Plateau and its surroundings, Global and Planetary Change, 68, 164-174, 2009.

Mcguire, C. R., Nufio, C. R., Bowers, M. D., and Guralnick, R. P.: Elevation-dependent temperature trends in the Rocky Mountain Front Range: changes over a 56- and 20-year record, PLOS ONE, 7, e44370, 2012.

Pepin, N., Deng, H., Zhang, H., Zhang, F., Kang, S., and Yao, T.: An examination of temperature trends at high elevations across the Tibetan Plateau: the use of MODIS LST to understand patterns of elevation-dependent warming, Journal of Geophysical Research, 124, 5738-5756, 2019.

Rangwala, I., Barsugli, J., Cozzetto, K., Neff, J. and Prairie, J.: Mid-21st century projections in temperature extremes in the southern Colorado Rocky Mountains from regional climate models, Climate Dynamics, 39, 1823-1840, 2012.

Rangwala, I., Miller, J. R., and Xu, M.: Warming in the Tibetan Plateau: possible influences of the changes in surface water vapor, Geophysical Research Letters, 36, L06703, 2009.

Rangwala, I., and Miller, J. R.: Climate change in mountains: a review of elevation-dependent warming and its possible causes, Climatic Change, 114, 527-547, 2012.

Seidel, D. J., and Free, M.: Comparison of lower-tropospheric temperature climatologies and trends at low and high elevation radiosonde sites, Climatic Change, 59, 53-74, 2003.

Simmons, A. J., Willett, K. M., Jones, P. D., Thorne, P. W., and Dee, D. P.: Low-frequency variations in surface atmospheric humidity, temperature, and precipitation: Inferences from reanalyses and monthly gridded observational data sets, Journal of Geophysical Research: Atmospheres, 115, D01110, doi:10.1029/2009jd012442, 2010.

Shi, Y., Liu, C., and Kang, E.: The glacier inventory of China, Annals of Glaciology, 50, 1-11, 2009.

Shi, T. L., Pu, W., Zhou, Y., Cui, J. C., Zhang, D. Z., and Wang, X.: Albedo of Black Carbon-Contaminated Snow Across Northwestern China and the Validation With Model Simulation, Journal of Geophysical Research: Atmospheres, 125, 2020.

Sorg, A., Bolch, T., Stoffel, M., Solomina, O. N., and Beniston, M.: Climate change impacts on glaciers and runoff in Tien Shan (Central Asia), Nature Climate Change, 2(10), 725-731, 2012.

Thakuri, S., Dahal, S., Shrestha, D., Guyennon, N., Romano, E., Colombo, N., and Salerno, F.: Elevation-dependent warming of maximum air temperature in Nepal during 1976–2015, Atmospheric Research, 228, 261-269, 2019.

Wang, K. C., Wang, P. C., Liu, J. M., Sparrow, M., Haginoya, S., and Zhou, X. J.: Variation of surface albedo and soil thermal parameters with soil moisture content at a semi-desert site on the western Tibetan Plateau, Boundary-Layer Meteorology, 116(1), 117-129, 2005.

Wang, P., Tang, G., Cao, L., Liu, Q., and Ren, Y.: Surface air temperature variability and its relationship with altitude and latitude over the Tibetan Plateau in 1981-2010, Advances in Climate Change Research, 8, 313-319, 2012. (in Chinese)

Wang, Q., Fan, X., and Wang, M.: Recent warming amplification over high elevation regions across the globe, Climate Dynamics, 43, 87-101, 2014.

Wang, S.S., Grant, R.F., Verseghy, D.L., and Black, T.A.: Modelling carbon dynamics of boreal forest ecosystems using the Canadian Land Surface Scheme, Climatic Change, 55(4), 451-477, 2002.

Zhang, C., Lu, D., Chen, X., Zhang, Y., Maisupova, B., and Tao, Y.: The spatiotemporal patterns of vegetation coverage and biomass of the temperate deserts in Central Asia and their relationships with climate controls, Remote Sensing of Environment, 175, 271-281, 2016.

Zhang, Y. L., Kang, S. C., Sprenger, M., Cong, Z. Y., Gao, T. G., Li, C. L., Tao, S., Li, X. F., Zhong, X. Y., Xu, M., Meng, W. J., Neupane, B., Qin, X., and Sillanpaa, M.: Black carbon and mineral dust in snow cover on the Tibetan Plateau, The Cryosphere, 12(2), 413-431, 2018.

Xu, M., Kang, S., Wu, H., and Yuan, X.: Detection of spatio-temporal variability of air temperature and precipitation based on long-term meteorological station observations over Tianshan Mountains, Central Asia, Atmospheric Research, 203, 141-163, 2018.

Yan, L., andLiu, X.: Has climatic warming over the Tibetan Plateau paused or continued in recent years? Journal of Earth, Ocean and Atmospheric Sciences, 1, 13-28, 2014.

You, Q., Kang, S., Pepin, N., Flugel, W., Yan, Y., Behrawan, H., and Huang, J.: Relationship between temperature trend magnitude, elevation and mean temperature in the Tibetan Plateau from homogenized surface stations and reanalysis data, Global and Planetary Change, 71, 124-133, 2010.

Zhang, C., Lu, D., Chen, X., Zhang, Y., Maisupova, B., and Tao, Y.: The spatiotemporal patterns of vegetation coverage and biomass of the temperate deserts in Central Asia and their relationships with climate controls, Remote Sensing of Environment, 175, 271-281, 2016.

Zhang, Y. L., Kang, S. C., Sprenger, M., Cong, Z. Y., Gao, T. G., Li, C. L., Tao, S., Li, X. F., Zhong, X. Y., Xu, M., Meng, W. J., Neupane, B., Qin, X., and Sillanpaa, M.: Black carbon and mineral dust in snow cover on the Tibetan Plateau, The Cryosphere, 12(2), 413-431, 2018.

Table 1. Altitude groups over the CTMD.

	Altitude range (m)	Grid number
1	<500	3139
2	500–1000	30810
3	1000-1500	83018
4	1500-2000	70229
5	2000-2500	46545
6	2500-3000	43400
7	3000-3500	39579
8	3500-4000	28256
9	4000-4500	8789
10	4500-5000	1666
11	5000-5500	496
12	5500-6000	150
13	6000-6500	54
14	>6500	4

Table 2. Ratio (%) of sum of grids at different significance levels ($p < 0.1$, $p < 0.05$, and $p < 0.01$) to total grids (356133).

	Tmin	Tmean	Tmax
January	3.28	3.65	6.48
February	9.66	0.55	56.65
March	52.02	99.35	100.00
April	3.76	69.16	46.36
May	46.97	29.21	7.63
June	80.33	92.37	49.63
July	46.86	51.97	38.82
August	35.58	56.37	40.84
September	19.87	47.77	35.32
October	11.78	25.52	11.41
November	12.00	14.07	14.12
December	0.38	0.00	0.00

Table 3. Annual and seasonal temperature trends (°C $10a^{-1}$) in the CTM (based on the CTMD) and the whole continental China (WCC) and low-altitude areas (LCC) by excluding the CTM and the QTP from the WCC (both based on the CMA05) from 1979 to 2016.

	CTM			WCC			LCC		
	Tmin	Tmean	Tmax	Tmin	Tmean	Tmax	Tmin	Tmean	Tmax
Spring	**0.633*****	**0.522*****	**0.640*****	0.557***	0.513***	0.518***	0.543***	0.498***	0.505***
Summer	0.441***	0.342***	0.266**	0.472***	0.388***	0.378***	0.404***	0.336***	0.348***
Autumn	0.302	0.200*	0.270	0.551***	0.458***	0.420***	0.506***	0.411***	0.371***
Winter	0.014	-0.085	0.115	0.432***	0.361***	0.327***	0.333**	0.257	0.211
Annual	0.347***	0.245***	0.323***	0.503***	0.430***	0.411***	0.446***	0.376***	0.359***

Note: the bold and underlined value indicates a greater warming trend in the CTM than WCC and LCC. * denotes the significance level $p<0.1$, ** denotes the significance level $p<0.05$, and *** denotes the significance level $p<0.01$.

Table 4. Monthly temperature trends (℃ 10a^{-1}) in the CTM (based on the CTMD) and the whole continental China (WCC) and low-elevation areas (LCC) by excluding the CTM and the QTP from the WCC (both based on the CMA05) from 1979 to 2016.

	CTM			WCC			LCC		
	Tmin	Tmean	Tmax	Tmin	Tmean	Tmax	Tmin	Tmean	Tmax
January	-0.133	-0.269	-0.235	0.343 **	0.256	0.212	0.225	0.143	0.102
February	0.313	0.177	**0.605** **	0.558 ***	0.523 ***	0.549 **	0.486 **	0.456 *	0.475 *
March	**0.835** **	**0.818** ***	**1.339** ***	0.651 ***	0.672 ***	0.752 ***	0.661 ***	0.673 ***	0.738 ***
April	0.441	**0.537** ***	**0.664** *	0.547 ***	0.522 ***	0.516 ***	0.520 ***	0.503 ***	0.508 ***
May	**0.624** **	0.211	-0.082	0.475 ***	0.345 ***	0.284 ***	0.447 ***	0.317 ***	0.270 ***
June	**0.752** ***	**0.476** ***	**0.422** ***	0.516 ***	0.390 ***	0.344 ***	0.467 ***	0.348 ***	0.320 ***
July	0.227	0.331 ***	0.28	0.472 ***	0.411 ***	0.416 ***	0.402 ***	0.343 ***	0.359 ***
August	0.342	0.217 *	0.095	0.429 ***	0.363 ***	0.375 ***	0.343 ***	0.318 ***	0.363 ***
September	0.246	0.237	0.33	0.559 ***	0.486 ***	0.495 ***	0.517 ***	0.445 ***	0.456 ***
October	0.273	0.18	0.227	0.524 ***	0.434 ***	0.398 ***	0.496 ***	0.407 ***	0.372 **
November	0.386	0.183	0.252	0.569 ***	0.455 ***	0.368 **	0.503 ***	0.381 **	0.285
December	-0.137	-0.164	-0.025	0.394 ***	0.303 **	0.219	0.287 *	0.171	0.055

Note: the bold and underlined value indicates a greater warming trend in the CTM than WCC and LCC. * denotes the significance level $p<0.1$, ** denotes the significance level $p<0.05$, and *** denotes the significance level $p<0.01$.

Table 5. Monthly temperature trends (℃ 10a^{-1}) over different elevations based on the CTMD from 1979 to 2016.

	Tmin	Tmean	Tmax
January	0.039***	0.036***	0.037***
February	0.033***	0.012	0.008***
March	0.023	0.009**	0.017***
April	0.021***	-0.02***	**0.069****
May	-0.056***	-0.022***	-0.045***
June	-0.025***	0.007	-0.046***
July	0.0	-0.017**	-0.019**
August	-0.011	**0.037****	**0.023****
September	-0.006	**0.017****	**0.038****
October	-0.073***	-0.018***	**0.017****
November	-0.032***	-0.031***	-0.018***
December	0.064***	**0.006****	-0.018***

Note: the bold and underlined value indicates a warming trend at higher altitudes, rather than the whole altitude range. More details could be found in Figure 2 to 4 and Figure S1 to S12. * denotes the significance level $p<0.1$, ** denotes the significance level $p<0.05$, and *** denotes the significance level $p<0.01$.

Table 6. Relationship (R^2) of snow depth (cm) and monthly Tmin, Tmean and Tmax from 1979 to 2016.

	Tmin	Tmean	Tmax
January	0.021	0.098 *	0.109 **
February	0.031	0.050	0.103 *
March	0.399 ***	0.400 ***	0.033
April	0.003	0.076	0.008
May	0.086 *	0.104 *	0.012
June	0.194 ***	0.230 ***	0.095 *
July	0.081 *	0.108 *	0.016
August	0.047	0.242 ***	0.083 *
September	0.001	0.072	0.150 **
October	0.010	0.020	0.103 *
November	0.051	0.125 **	0.151 **
December	0.014	0.159 **	0.200 ***

Note: * denotes the significance level $p < 0.1$, ** denotes the significance level $p < 0.05$, and *** denotes the significance level $p < 0.01$.

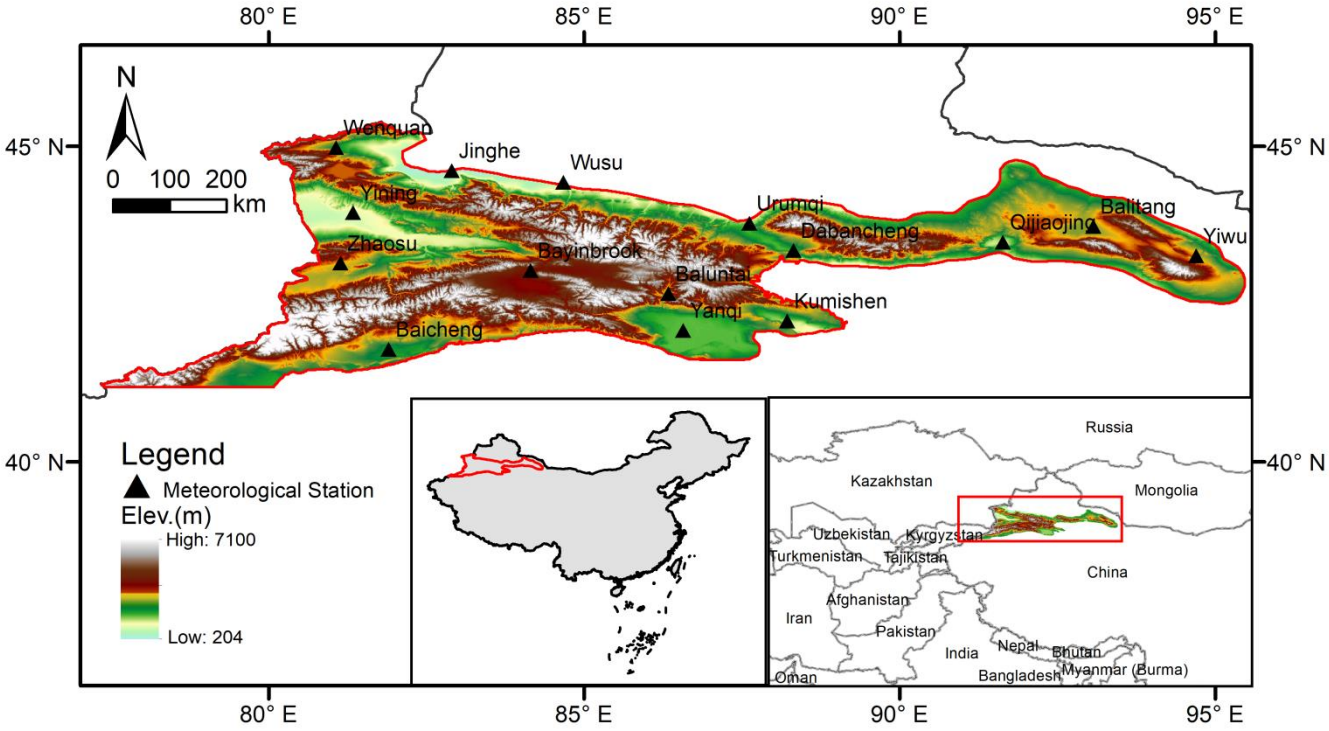

Figure1: Location of the Chinese Tianshan Mountains (CTM).The elevation ranges from 204 m to 7100 m a.s.l., with a DEM resolution of 1 km from SRTM. The grey sub-plot show the extent of the CMA05 at the 0.5 °×0.5 °grid.

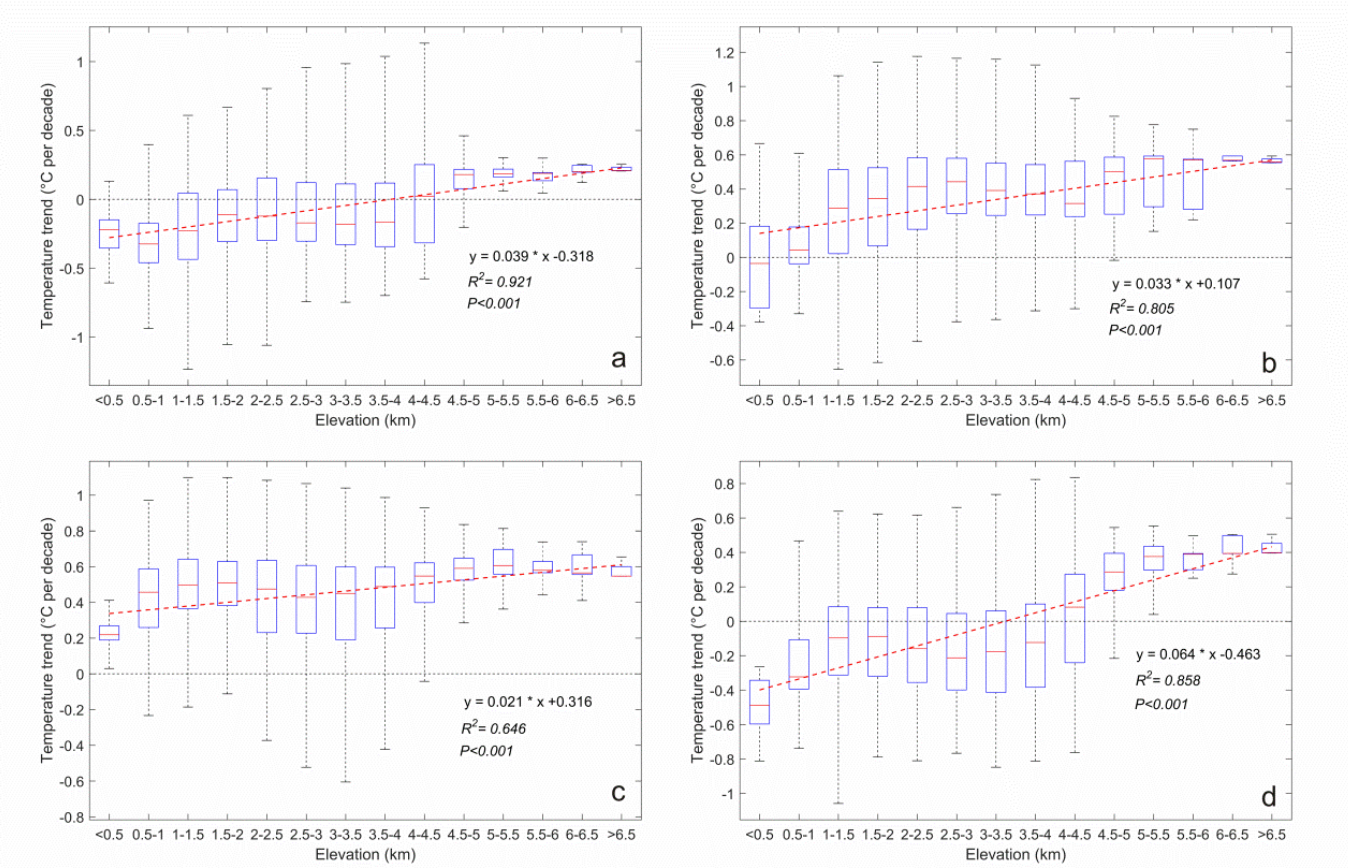

Figure 2: Box plots of monthly minimum temperature trends at different elevations from 1979 to 2016. (a) January, (b) February, (c) April, and (d) December. Thick horizontal lines in boxes show the median values. Boxes indicate the inner-quantile range (25% to 75%) and the whiskers show the full range of the values. The red dashed lines represent the significance of EDW.

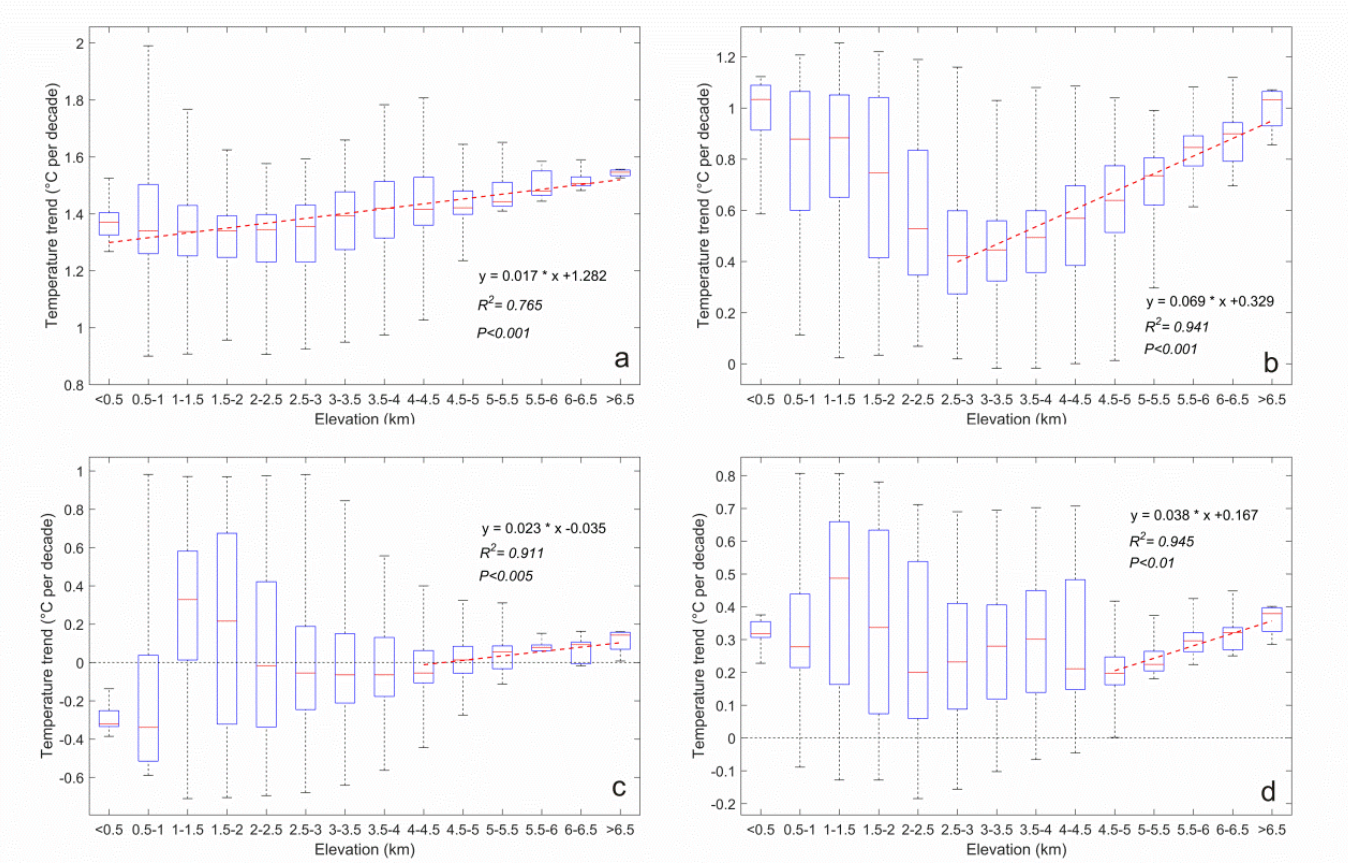

Figure 3: Box plots of monthly maximum temperature trends at different elevations from 1979 to 2016. (a) March, (b) April, (c) August, and (d) September. Thick horizontal lines in boxes show the median values. Boxes indicate the innerquartile range (25% to 75%) and the whiskers show the full range of the values. The red dashed lines represent the significance of EDW.

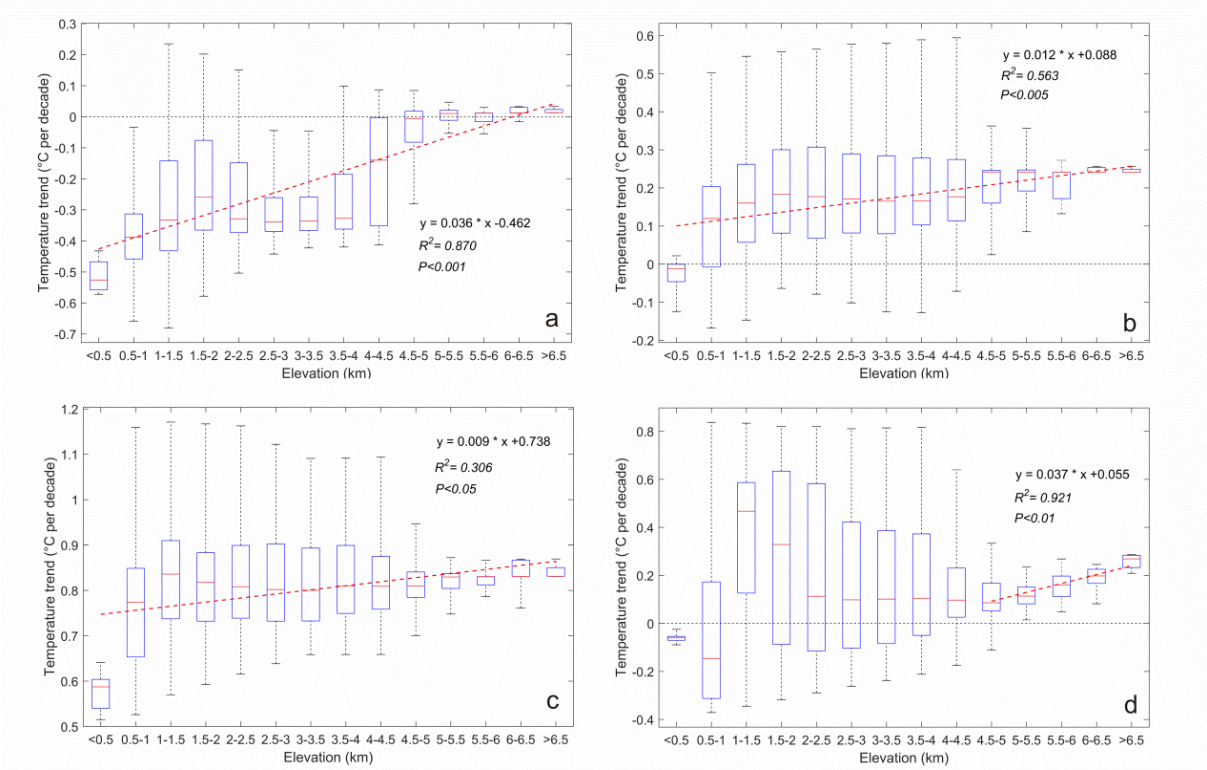

600 **Figure 4: Box plots of monthly mean temperature trends at different elevations from 1979 to 2016. (a) January, (b) February, (c) March, and (d) August. Thick horizontal lines in boxes show the median values. Boxes indicate the innerquartile (25% to 75%) and the whiskers show the full range of the values. The red dashed lines represent the significance of EDW.**

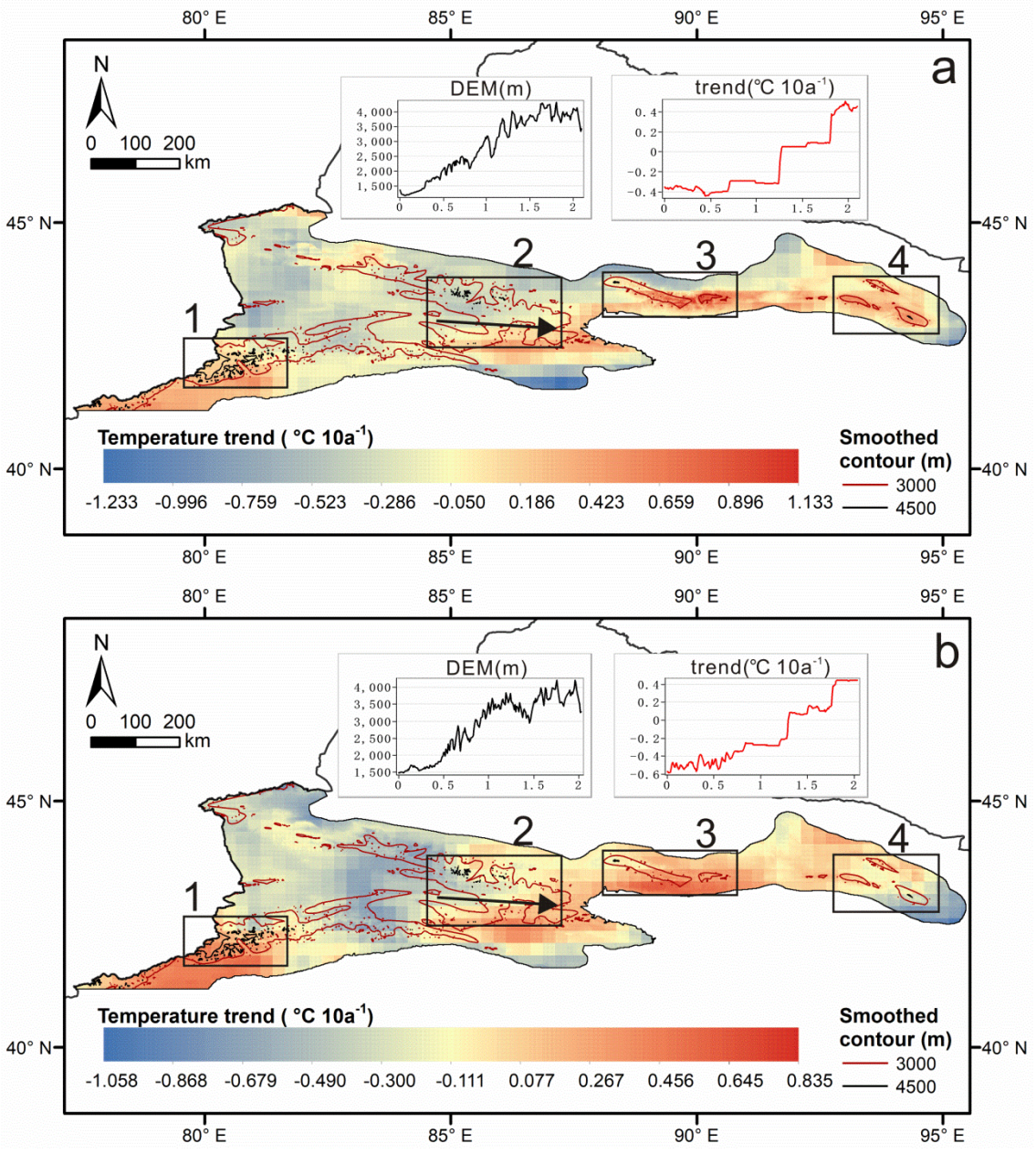

605

Figure 5: Monthly minimum temperature trends (a) January and (b) December for the entire CTM from 1979 to 2016. The ordinate of two sub-plots show the elevation trend and temperature trend along the terrain profile (black arrow indicates the direction) in Zone 2, respectively. The abscissa represents the distance in multiples of the scale.

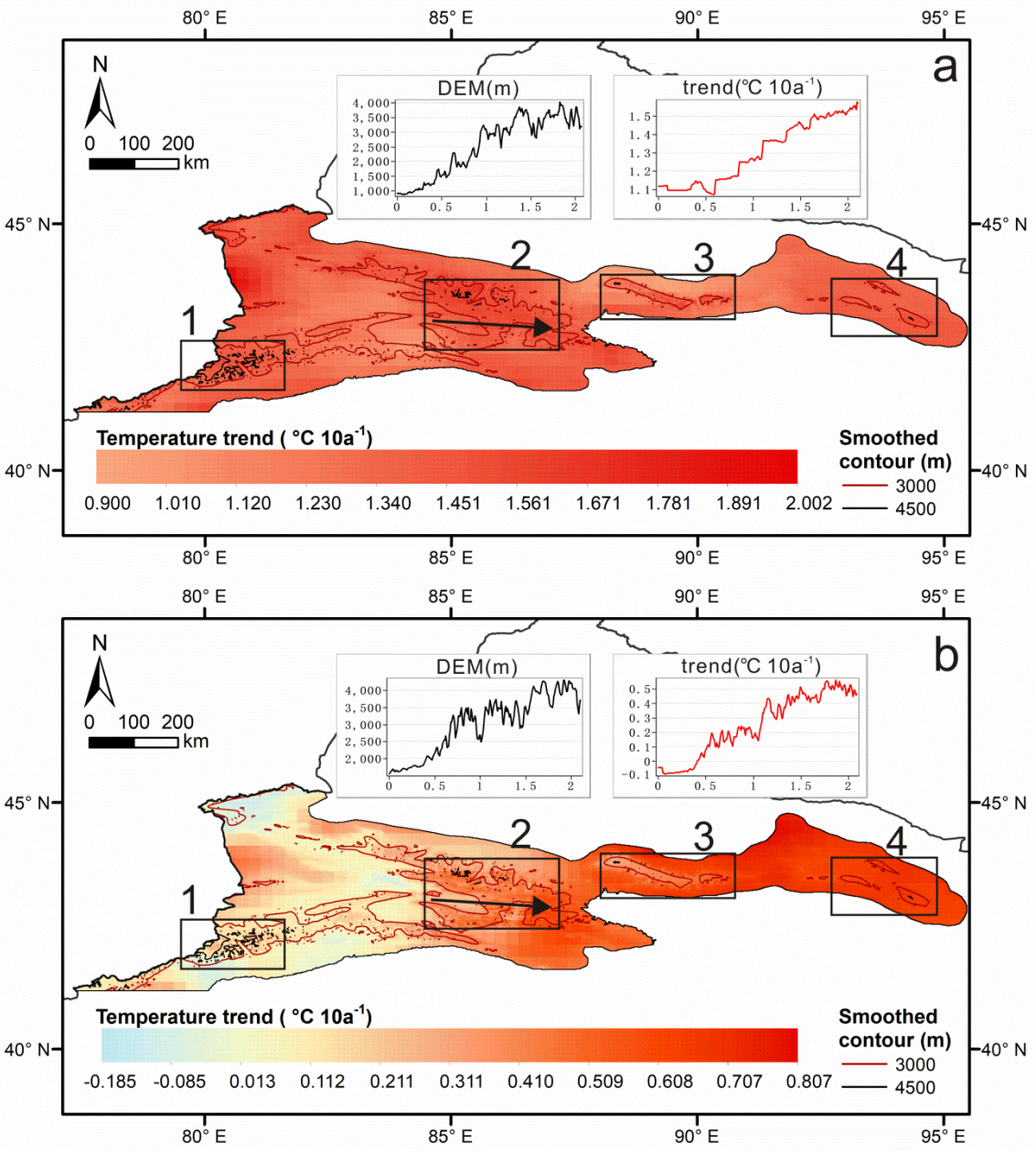

Figure 6: Monthly maximum temperature trends (a) March and (b) September for the entire CTM from 1979 to 2016. The ordinate of two sub-plots show the elevation trend and temperature trend along the terrain profile (black arrow indicates the direction) in Zone 2, respectively. The abscissa represents the distance in multiples of the scale.

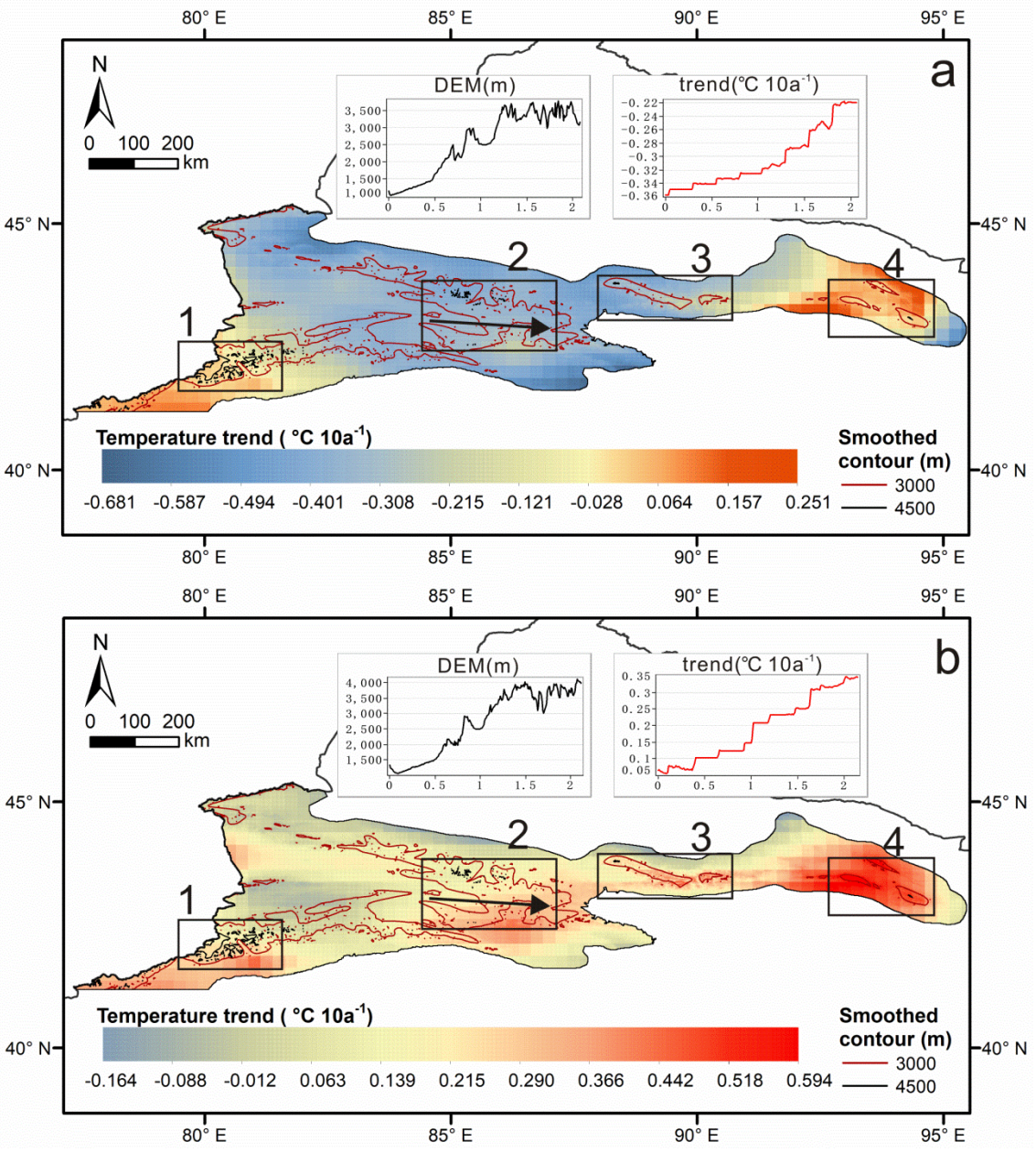

Figure 7: Monthly mean temperature trends (a) January and (b) February for the entire CTM from 1979 to 2016. The ordinate of two sub-plots show the elevation trend and temperature trend along the terrain profile (black arrow indicates the direction) in Zone 2, respectively. The abscissa represents the distance in multiples of the scale.

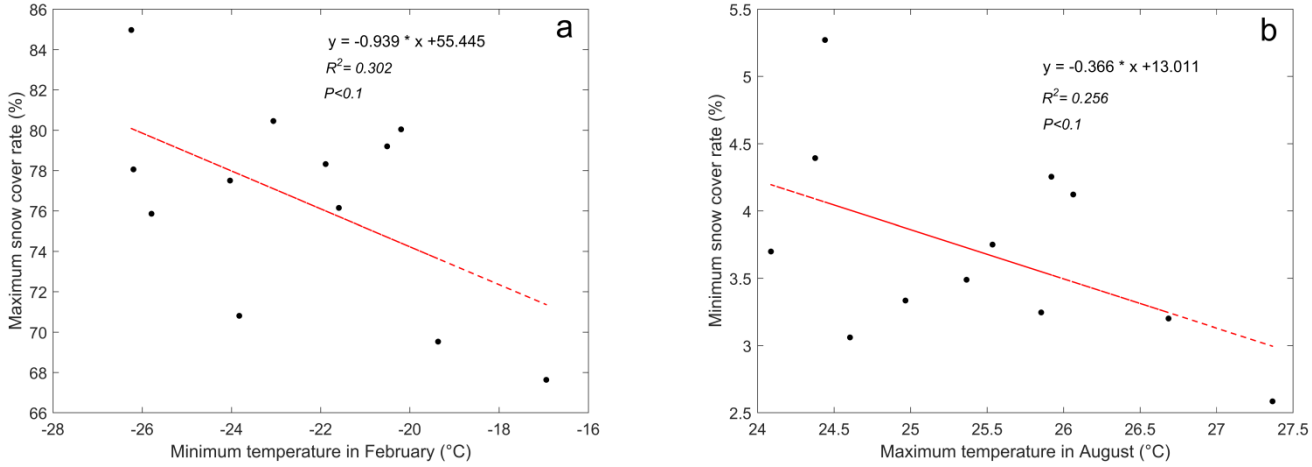

620

Figure 8: Relationship of temperature and snow cover rate (a) minimum temperature in February vs. maximum snow cover rate and (b) maximum temperature in August vs. minimum snow cover rate from 2002 to 2013.

625

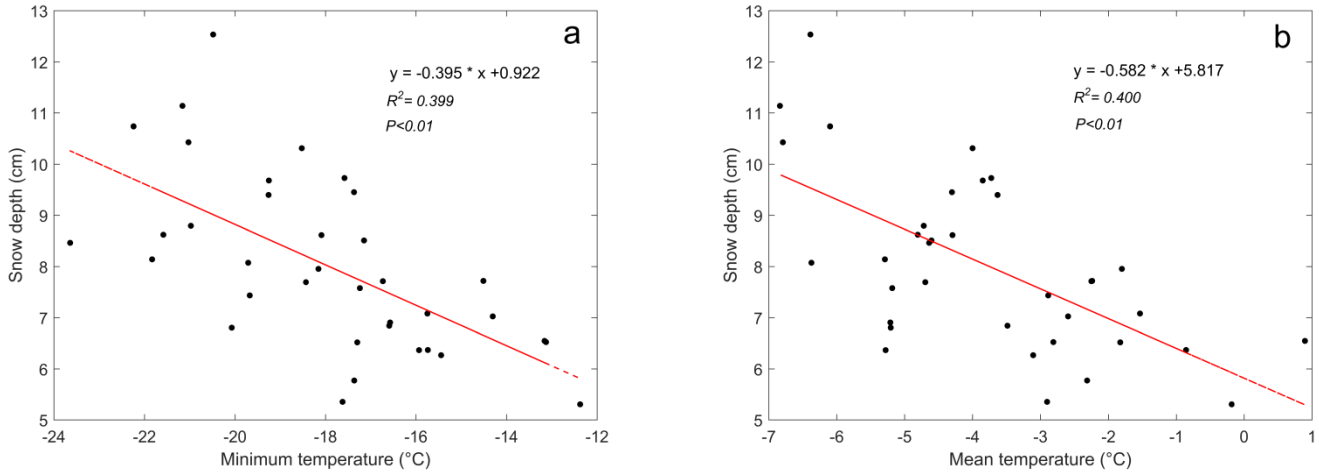

Figure 9: Relationship of snow depth and (a) Tmin in March and (b) Tmean in March from 1979 to 2016.